CrystEngComm

Accepted Manuscript

ROYAL SOCIETY OF CHEMISTRY

www.rsc.org/crystengcomm

CrystEngComm RSCPublishing

COMMUNICATION

Heterostructured Calcium Carbonate Nanowires Controlled by a Cationic Polyelectrolyte†

Cite this: DOI: 10.1039/x0xx00000x

Jianhua Zhu*, Lei Huang, Mingfang Cui, Li Ma

Received 00th xxx 2014,
Accepted 00th xxx 2014

DOI: 10.1039/x0xx00000x

www.rsc.org/CrystEngComm

The heterostructured biomimetic materials of calcite microcrystals covered with aragonite nanowires, as well as aragonite fibers decorated with small calcite tips, were first synthesized in a cationic polyelectrolyte mineral solution. The polymorph switching in the same microstructures shows close relationship with thermodynamic and kinetic reaction control.

Polymorph control is a key issue for natural biominerals, but it has shown to be difficult to reproduce in the lab, where polymorphic mixtures are often synthesized. Polymorph selection of calcium carbonate is usually achieved to a great extent in biological systems. Many organisms are capable of controlling over mineral polymorphs intelligently to construct functional biomaterials of inorganic-organic composite materials. For instance, the fish otoliths, as useful biogenetic biominerals for gravity sensing and perception of sound, are composed of calcium carbonate (aragonite, calcite and vaterite) and organic matrices. These different polymorphs contain low Mg^{2+} ingredient and are stable in both freshwater and marine fishes. Their formation is considered to be regulated by macromolecules, but not by special ionic microenvironment.[1] The mollusk shell, a typical hard tissue with extraordinarily mechanical performance, is also a heterogeneous composite consisting of organic matrices, calcite and aragonite crystallites. They were reported to be in vivo induced by calcite- and aragonite-related proteins, respectively.[2] Knowledge underlying the phase transition, morphology change and architecture formation is still controversial a biogenic materials, but it is acceptable that organic matrices (soluble or insoluble) play an important role during their formation.

So far, many strategies have been applied to regulate crystalline phases, invovling changing temperatures,[3] solvents,[4] agitation,[5] organic substrate[6] and other reaction condition.[7] The use of synthetic polymer also offers a versatile routine to modulate polymorph and morphology of inorganic minerals.[8] Recently, Wang *et al.* represented the heterostructured $CaCO_3$ microspheres with calcite loops and vaterite spherical cores using mixed additives of poly(sodium 4-styrenesulfonate) and folic acid.[9] Liu *et al.* addressed synthesis of calcite and aragonite complex layered material using Mg^{2+} to induce the growth of aragonite layer.[10] Until now, synthesis of more than one $CaCO_3$ polymorph in the same micro-/nano-structures is still a great challenge in vitro study when a single additive is used.

Herein, we report the fascinating $CaCO_3$ heterostructures, including aragonite nanowires (NWs) growing on calcite microcrystals and the continuously developed superstructures with rhombohedral calcite tips. To the best of our knowledge, it is the first example to produce the aragonite/calcite heterostructures only utilizing a positively charged polyelectrolyte poly(allylamine hydrochloride)(PAH) to date. Our research collaborates that the $CaCO_3$ polymorph switching from calcite to aragonite, or the opposite case, can be successfully realized within an individual microstructure by changing the solute concentrations and spatial distribution of polymer in the microenvironments.

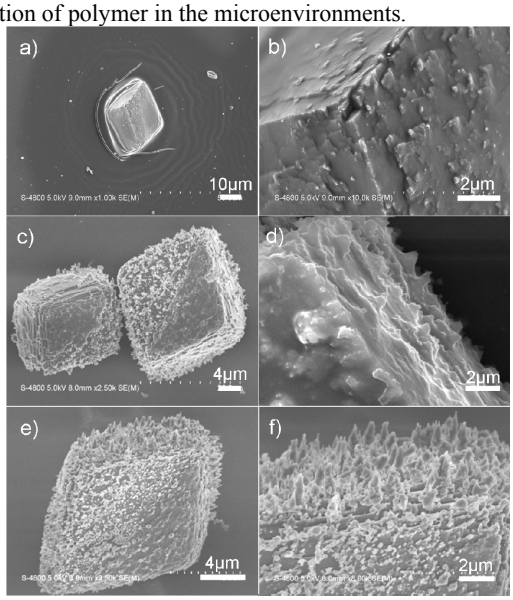

Fig. 1 (a-b) SEM images of the calcite crystal and the mineral coatings in the dissolution process; (c-d) the re-crystallization process in a gas diffusion procedure after 1 day, [$CaCl_2$]=2mM; (e-f) after 2-3 day.

Initially, well-defined rhombohedral calcite crystals were introduced in the PAH (0.1g/L) solution under air atmosphere. The

positively charged polymer contains $-NH_3^+$ groups in the side chains, which can effectively interact with carbonate ions on the [104] planes. Carbonate ions are first released from the crystal faces, and then calcium ions follow. Classical layer-by-layer dissolution of crystals occurred and produce obvious terraces (Fig. 1b-c). After one day, gelatinous mineral films were observed on the crystal surface and glass slices (Fig. 1a-b). They could form concentric ring patterns around the microcrystals resembling Liesegang rings.[11] The energy dispersive X-ray spectroscopy (EDX) analysis (Fig. S1, ESI†) revealed that the films contain a great deal of polymer because of high mole ratio of C/Ca (1.9:1). Considering the dissolution process, it is certain that the gelatinous coatings are highly hydrous mineral intermediates composed of PAH/CO_3^{2-}/Ca^{2+} in analogy to those acidic polymer-induced liquid-precursor (PILP) phases. [12] **Error! Bookmark not defined.** Recently, Meldrum and coworkers also reported the analogous liquid mineral precursor produced via a microphase separation induced by PAH.[13] They domonstrated that calcium ions could be partly replaced by positively polyelectrolyte molecules in the liquid mineral precursor. However, in the current case the mineral precursor formed in the dissolution process rather than the gas diffusion procedure. Additionally, annular patterns were produced probably due to the cyclic variation of solute concentrations around calcite crystals caused by the disintegration or dissolving of the mineral precursor.

After one day, a little amount of $CaCl_2$ was replenished which can slow down the crystal dissolution rate, and simultaneously initiate the crystallization process under the gas diffusion procedure (NH_3 and CO_2). Gelatinous nanoshoots appeared on the surface of calcite substrate crystals (Fig. 1c-d). After 2-3 days, they kept growing into arrayed tapers (Fig. 1e-f). SAED pattern proved that they were still in polycrystalline state (Fig. S4a, ESI†).

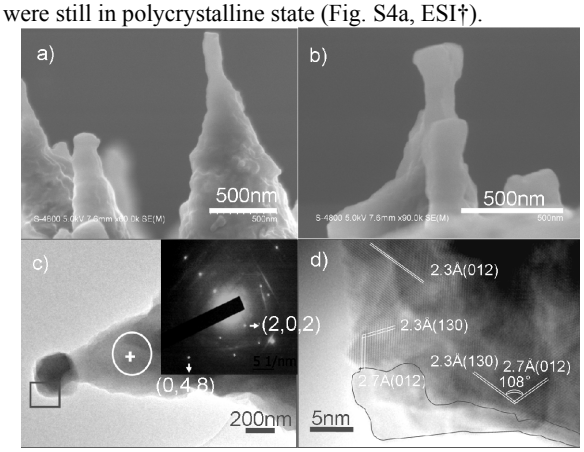

Fig. 2 (a) SEM images of growing nanorods after 5 days; (b-c) SEM and TEM images of nanorods with irregular growing points, inset showing SAED pattern of the lower taper; (d) HRTEM image of the tip.

Subsequently, notable short rods were seen to originate from lower tapers after crystallization for 5 days (Fig. 2a and Fig. S2, ESI†). A few rods were terminated with "bobbles" or droplets[14] at their tips (Fig. 2b-c), which was very similar with the SPS (solution-precursor-solid) process[15] caused by the anionic polyelectrolyte. In the present case, the droplet-like growing points were actually induced by the cationic polyelectrolyte PAH. XRD pattern reveals that aragonite phase occurs besides the calcite substrate (Fig. S3, ESI†). The tips of rods are further analyzed by HRTEM (Fig. 2d), which exhibits fringe lattice of 2.70Å corresponding to the (012) planes of aragonite. They are still in a nanoparticulate substructure with a random arrangement. The amorphous edges marked by the irregular curve indicate that nanoparticles (NPs) in the growing points are actually developed from the amorphous calcium carbonate (ACC). SAED study of the lower tapers do not present a typical single pattern as some messy points appear (inset in Fig. 2c), but their major growth direction is along [012]. Other nanorods grow with swelled tips (Fig. S4b, ESI†). And selected area diffraction reveals that they comprise polycrystalline aragonite NPs.

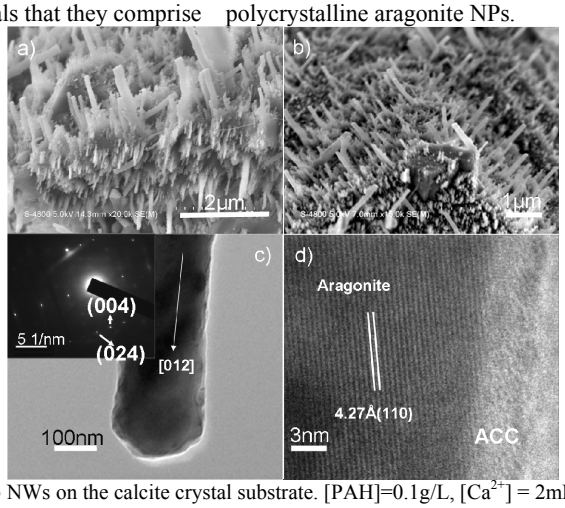

Fig. 3 NWs on the calcite crystal substrate. [PAH]=0.1g/L, [Ca^{2+}] = 2mM. (a-b) SEM image of NWs on different surfaces of calcite crystals, after 14 days; (c) TEM image and its SAED pattern; (d) HRTEM image.

Long and dense NWs deposit on different faces of the substrate crystals with prolonged time, which are predominantly perpendicular to the calcite surface (Fig. 3a-b and Fig. S5, ESI†). Gelatinous mineral coatings could be observed distinctly in the root of NWs, which was an obvious indication of heterogeneous nucleation process. A typical analysis of a wire was presented in Fig. 3c. The relative ED pattern can be indexed as an aragonite single crystal with the growth direction along [012]. HRTEM image further confirms that it has a well crystallized aragonite core sheathed by an ACC layer (~ 4nm, Fig. 3d).[16] A similar layer was found on the aragonite platelets of nacre[17]and other synthetic aragonite.[18] Presumably this amorphous "coating" may work as a protective coating,[19] restraining aragonite against transformation or re-crystallization in the solution.

It has been demonstrated that the positively charged polyelectrolyte with amine side groups could effectively promote the vaterite formation. [20] A linear poly(ethylenimine) with low molecular weight (<2000) was reported to regulate the aragonite crystal growth at the air-water interface.[21] Recently, PAH has proven extremely effective to direct formation of calcite/vaterite thin films and calcite fibers.[22] As far as we know, PAH has never been reported to induce formation of the metastable aragonite crystals. Cölfen *et al.* ever reported the "sheaf bundle" aragonite superstructures using a hydrophilic block copolymer.[23] Xu *et al.* also demonstrated the synthesis of three $CaCO_3$ polymorphs using a single copolymer. [24] They all corroborated that low reactant concentrations and heterogeneous nucleation process favored the aragonite formation. Considering the present experiments, the formation of early gelatinous mineral coatings has consumed a great deal of Ca^{2+} and polymer (Fig. S7, ESI†). The low solute concentration can not promote formation of calcite crystals. Nevertheless, it favors the heterogeneous aragonite nucleation to produce NWs.

Control experiments were performed to investigate impacts of the polymer concentrations on the $CaCO_3$ polymorph switching. It has been confirmed that PAH should be kept in low concentration ranges to produce aragonite NWs (≤0.2g/L). When PAH increased to a high concentration ([PAH]=0.25g/L), there were about 40% calcite NWs among the aragonite crystals (Fig. S6, ESI†). At [PAH] = 5g/L, the major products were ultralong calcite wires (Fig. 4c and Fig. S7, ESI†). Evidently, calcite crystals favorably came into being at high

polymer concentrations. Kitano method has proven that PAH is a strong nucleation inhibitor for crystallization at high concentrations (Fig. S9, ESI†). This means that the crystallization from amorphous precursor is slowed down, thus shifting the reaction to the thermodynamically stable product of calcite, until the amorphous phase is almost consumed.

In contrast, aragonite forms at very low polymer concentrations as crystallization is less inhibited. The solution facilitates the kinetic rather than thermodynamic process. Few amorphous NPs are present in the solution, and it lowers the absolute nucleation rate as well as the probability of particle-particle growth events. In such a situation, heterogeneous nucleation on the gelatinous coating is energetically favored over homogeneous nucleation, as aragonite crystals in general cannot homogeneously nucleate under standard conditions.

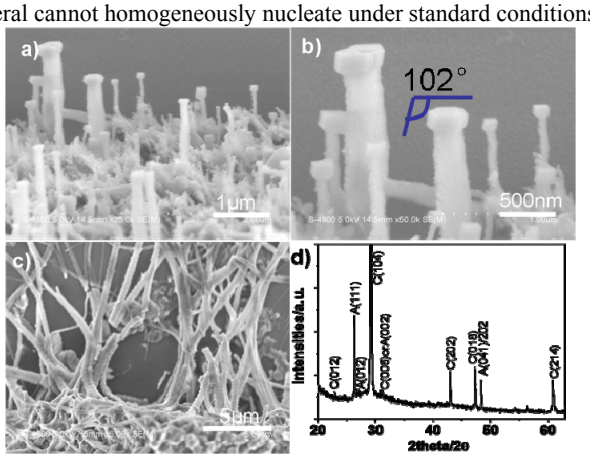

Fig. 4 (a-b) The bolt-like NWs.(c) The ultralong nanofibers. (d) XRD pattern of samples in (a), calcite and aragonite peaks are labeled as "C" and "A", respectively.

Interestingly, other fascinating $CaCO_3$ superstructures are observed in the mineral solution (Fig. 4a-b). SEM images show that they are NWs terminated with regular rhombohedron tips (100-300nm). The angles between two adjacent planes of the polyhedral tips are about 102°, which are consistent with calcite rhombohedron crystals. At the same time, nanopillars may correspond to aragonite NWs. The morphological change within an individual microstructure means that the polymorph switching may take place. Additionally, XRD pattern has signals of aragonite crystals coexisting with calcite phase. Following HRTEM analysis will further corroborate above presumption.

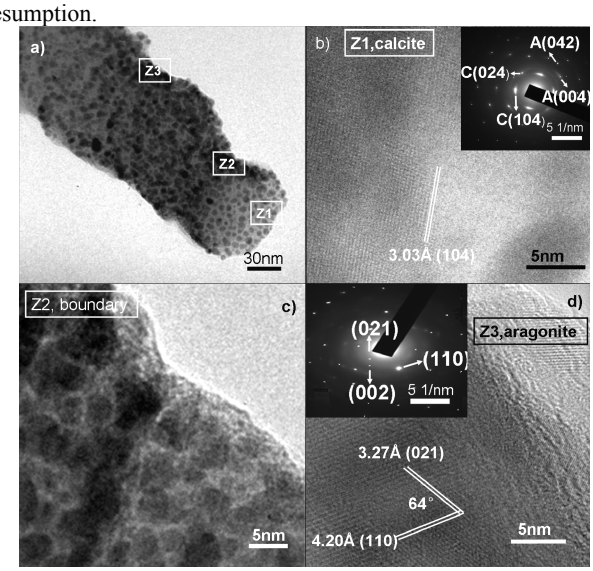

Fig. 5 TEM and HRTEM images of a heterostructured $CaCO_3$ NW. (a) TEM image; (b) HRTEM image of the upper tip (Z_1); (c) the boundary zone (Z_2); (d) the lower fibrous structure (Z_3).

Fig. 5a shows the typical TEM image of a bolt-like NW. HRTEM image of Z_3 region reveals the resolved lattice fringes of 4.20Å and 3.27Å, which is in good agreement with (110) and (021) planes of aragonite, respectively. The corresponding SAED analysis shows the same result (inset in Fig. 5d). However, HRTEM analysis of the Z_1 nanoregion definitely manifests that the polyhedral tip is a calcite crystal in the form of mesocrystals (Fig. 5b). The amorphous layer on the edges means that the rhombohedron tips also grow via the ACC intermediate. The relevant SAED result displays a typical calcite pattern associated with few aragonite planes of lower fibrous domains. Surprisingly, the Z_2 boundary shows amorphous property without any discernible lattice fringes (Fig. 5c). Therefore, upper calcite tips actually form based on the ACC layer via a heterogeneous nucleation process. The variation of reaction condition leads to calcite instead of aragonite NPs form within the growing points, where rhombohedron tips grow via a mesoscale self-assembly.

It has been reported that solid phase transition of aragonite to calcite was kinetically unlikely due to much higher activation energies (234.5±5.6kJ/mol), [25] although this process is thermodynamically favorable because of low Gibbs free energy in pure water (0.4kJ/mol).[26] Therefore, above transformation can only take place in a solution-based process. In such condition, nucleation and crystal growth kinetics are the crucial factors to manipulate $CaCO_3$ polymorphs. Analysis shows that concentrations of calcium ions and polymer decrease greatly in the final stage of mineralization (Fig. S7). Generally speaking, it is very suitable for growth of aragonite crystals. Now that formation of calcite tips is clearly identified, the question arises on the mechanism underling the polymorph switching from aragonite to calcite.

The preliminary analysis shows that the C/Ca ratios of aragonite NWs increase dramatically close to the growing points (Fig. S10a-b, ESI†). Evidently, PAH molecules will gradually accumulate onto the growing points during growth of wires. To further determine the spatial distribution of polymer molecules, fluorescent molecules of 1-pyrenecarboxaldehyde (Py-CHO) were used to treat with the preformed NWs (Fig. S10, ESI†). As Py-CHO molecules can easily react with the $-NH_2$ groups in PAH molecules, they can tag the polyelectrolyte by forming Schiff base. [27] The confocal laser scanning microscopy (CLSM) image shows that the fluorescent signal at the end of NWs is greatly enhanced (Fig. S10c, ESI†), which means that PAH molecules markedly accumulate on the tips of NWs. Additionally, EDX study reveals more polymer molecules are detected on the bolt-like NWs than the simple aragonite fibers. Therefore, the polymer accumulation at the fibrous tips must be a crucial factor influencing the polymorph selection. Initially, low PAH concentrations favor formation of aragonite NPs on the tips. But this process simultaneously results into more polymer aggregation at growing points. When its concentration reaches to a critical level, the tips become more suitable for formation of calcite rather than aragonite NPs. The kinetic control gives way to the thermodynamic process, and heterogeneous calcite nucleation will happen naturally. Once calcite nanoparticle seeds have formed, they will assemble into the mesocrystalline calcite superstructure. Meanwhile, formation of half or partial rhombohedrons on the tops of NWs means that growth of calcite tips is also influenced by the concentration of carbonate and calcium ions in the microenvironment (Fig. S7b, ESI†).

Conclusions

Briefly, polymorph switching from calcite to aragonite, and the

opposite case, could be successfully realized via spontaneous variations of solute in bulk solution and spatial distribution control of polymer in the microenvironment. Our finding opens new opportunities for designing novel heterostructured biomimetic minerals by elaborately controlling thermodynamic and kinetic reaction.

This work was supported by the Natural Science Foundation of China (Grant No. 21101004).

Notes and references

Anhui Province Key Laboratory of Metallurgical Emission Reduction & Resources Recycling, Anhui University of Technology, Maanshan, Anhui, China. Email: thesea@ustc.edu.cn.

†Electronic supplementary information (ESI) available: Full description of experimental methods, and supplementary data and figures. See DOI: 10.1039/c000000x/.

1 H. Tohse, K. Saruwatari, T. Kogure and H. Nagasawa, Y. Takagi, *Cryst. Growth & Des.*, 2009, **9**, 4897.
2 G. Falini, S. Albeck, S. Weiner and L. Addadi, *Science*, 1996, **271**, 67.
3 Q. Q. Yang and Z. D. Nan, *Mater. Res. Bull.*, 2010, **45**, 1777.
4 S. F. Chen, S. H. Yu, J. Jiang, F. Q. Li and Y. K. Liu, *Chem. Mater.*, 2006, **18**, 115.
5 J. X. Jiang, Y. Zhang, D. D. Xua and J. N. Liu, *CrystEngComm.*, 2014, **16**, 5221.
6 F. J. Zhu, T. Nishimura, H. Eimura and T. Kato, *CrystEngComm.*, 2014, **16**, 1496.
7 Y. X. Gao, S. H. Yu, H. P. Cong, J. Jiang, A. W. Xu, W. F. Dong and H. Cölfen, *J. Phys. Chem. B*, 2006, **110**, 6432.
8 S. Shi, Z. Su, H. Wei and X. Chen, *J. Appl. Polym. Sci.*, 2010, **117**, 3308.
9 S. S. Wang, A. Picker, H. Cölfen and A. W. Xu, *Angew. Chem. Int. Ed.,* 2013, **52**, 6317.
10 R. Liu, X. R, Xu, Y. R. Cai, A. H. Cai, H. H. Pan, R. K. Tang and K. W. Cho, *Cryst. Growth & Des.*, 2009, **9**, 3095.
11 R. E. Liesegang, *Naturwiss. Wochenschr.*, 1896, **11**, 53.
12 M.J. Olszta, Odom D J, Douglas E P, Gower L B, *Connect. Tissue Res.*, 2003, **44**, 326.
13 B. Cantaert, Y. Y. Kim, H. Ludwig, F. Nudelman, N. A. J. M. Sommerdijk and F. C. Meldrum, *Adv. Funct. Mater.*, 2012, **22**, 907.
14 J. H. Zhu, S. H. Yu, A. W. Xu and H. Cölfen, Chem. Commun., 2009, 1106.
15 M. J. Olszta, S. Gajjeraman, M. Kaufman and L. B. Gower, *Chem. Mater.,* 2004, **16**, 2355.
16 N. Nassif, N. Pinna, N. Gehrke, M. Antonietti and C. Jäger, H. Cölfen, *PNAS*, 2005, **102**, 12653.
17 N. Nassif, N. Pinna, N. Gehrke, M. Antonietti, C. Jäger and H. Cölfen, *Proc. Natl. Acad. Sci.*, USA 2005, **102**, 12563.
18 Z. Q. Huang and Gangsheng Zhang, *Cryst. Growth Des.*, 2012, **12**, 1816.
19 N. Nassif, N. Gehrke, N. Pinna, N. Shirshova, K. Tauer, M. Antonietti and H. Cölfen, *Angew. Chem. Int. Ed.*, 2005, **44**, 6004.
20 A. W. Xu, M. Antonietti, H. Cölfen and Y. P. Fang, *Adv. Funct. Mater.*, 2006, **16**, 903.
21 H. K. Park, I. Lee and K. Kim, *Chem. Commun.*, 2004, **1**, 24.
22 B. Cantaert, A. Verch, Y. Y. Kim, H. Ludwig, V. N. Paunov, R. Kröger and F. C. Meldrum, *Chem. Mater.*, 2013, **25**, 4994.
23 N. Nassif, N. Gehrke, N. Pinna, N. Shirshova, K. Tauer, M. Antonietti and H. Cölfen, *Angew. Chem. Int. Ed.*, 2005, **44**, 6004.
24 A. W. Xu, W. F. Dong, M. Antonietti and H. Cölfen, *Adv. Funct. Mater.*, 2008, **18**, 1307.
25 J. Peric, M. Vucak, R. Krstuovic, L. Brecevic, D. Kralj, *Thermochim. Acta*, 1996, **27**, 175.
26 G. Wolf, C. Günther, *J. Therm. Anal. Calorimetry*, 2001, **65**, 687.
27 Z. P. Wang, H. Mohwald, C. Y. Gao, *ACS nano*, 2011, **5**, 3930.

